Electronic structure of the GaAs:Mn_{Ga} center

M. Linnarsson,* E. Janzén, and B. Monemar
Department of Physics and Measurement Technology, Linköping University, S-581 83 Linköping, Sweden

M. Kleverman and A. Thilderkvist
Department of Solid State Physics, University of Lund, Box 118, S-221 00 Lund, Sweden

(Received 3 June 1996; revised manuscript received 12 November 1996)

The excitation spectrum of the 0.11-eV Mn acceptor in GaAs has been thoroughly investigated by uniaxial stress and Zeeman fourier transform infrared spectroscopy. The results give strong evidence for the $3d^5$+shallow hole model for the Mn^0 center. The deformation potentials as well as the g values determined for the hole are in close agreement with those previously reported for the $1S_{3/2}(\Gamma_8)$ state for shallow acceptors in GaAs. All experimental results are in accordance with a $J=1$ ground-state level derived from exchange coupling of the shallow $1S_{3/2}(\Gamma_8)$ hole and the $S=5/2$ Mn^- core. A splitting between $J=2$ and $J=1$ levels in the range from 9 to 12 meV is inferred and is considerably larger than the 2–3 meV splitting previously suggested [S0163-1829(97)01411-2]

I. INTRODUCTION

Mn and GaAs gives rise to an acceptor level at about 0.113 eV above the valence band. It has been studied by various techniques, e.g., Hall measurements,[1] photoluminescence,[2,3] absorption,[4,5] and space-charge techniques.[6] The absorption spectrum is very similar to those observed for more shallow acceptor levels in GaAs with respect to, e.g., the energy spacing between the excited states for the Mn acceptor, but it is shifted to higher energies due to the considerably large ground-state energy. The final states in the optical transition have been identified as shallow acceptor states well described within the effective-mass approximation (EMA). Atomic manganese has an $[Ar]3d^54s^2$ configuration and on a Ga site three electrons are needed for completing the bonds with the nearest As atoms. In this way a $3d^4$ ground-state configuration could be inferred for Mn^0 with a $^5T_2$ ground-state term. A spectrum characteristic for $^{55}Mn^-$ was observed in electron paramagnetic resonance (EPR) (Refs. 7 and 8) with an isotropic hyperfine spectrum. For Mn^0, EPR (Ref. 9) and microwave circular dichroism (MCD) (Ref. 10) results suggest an alternative model in which the Mn^0 ground-state configuration is $3d^5(Mn)^-$+(shallow hole) rather than $3d^4$. This model is also supported by recent Zeeman results.[5] The experimental data to be presented here give additional strong evidence for the $3d^5$+(shallow hole) model and also identify the $J=1$ level as the ground state.

The excitation spectrum of Mn^0 will, in this paper, be analyzed using the Mn^-+(shallow hole) model. The model employed is as follows. The shallow hole is bound to the Mn^- ion by the Coulomb potential, while both subsystems, i.e., the hole and the core, basically retain their electronic structure. Mn^- has a $3d^5$ configuration and, according to Hund's rule, a $^6A_2$ ground-state term. The direct and exchange Coulomb interactions between the two subsystems are strongly dependent on the overlap between the hole and the core wave functions. A noticeable exchange interaction is therefore expected only for those hole states that have a nonvanishing amplitude at the origin, i.e., the S-like states in generally, and for the $1S_{3/2}(\Gamma_8)$ hole state in particular. It has been established that the observed excitation spectrum is due to hole transitions from the $1S_{3/2}(\Gamma_8)$ state in the coupled ground state to excited P-like states. The interaction between the hole in a P-like state and the core is expected to be small, which is in accord with the experimental findings in which no such interaction has been detected. We therefore conclude that the exchange interaction only has to be taken into account for the initial state in the transitions.

The Mn^- core behaved as an $S=5/2$ state (spherical approximation) and the hole in the $1S_{3/2}(\Gamma_8)$ state is characterized by an effective angular momentum $j=3/2$. In the jj-coupling scheme, the exchange interaction takes the form $H_{\text{exchange}}=J\mathbf{S}\cdot\mathbf{j}$. The constant of motion is the total effective angular momentum $\mathbf{J'=j+S}$. The Mn^0 ground-state term splits into levels with an effective angular momentum $J'=1$, 2, 3, and 4 with energies 0, $2J$, $5J$, and $9J$, respectively, and the $J'=1$ is expected to be the ground state.[9] The levels with $J'\geqslant 2$ will generally split in their irreducible components, but it is expected that such a splitting is much smaller than the J' level splitting and could therefore be neglected. The nth coupled core-hole state $|nSjJ'M_{J'}\rangle$ is, in the jj-coupling scheme, given by

$$|nSjJ'M_{J'}\rangle=\sum_{m_S,m_j}(SM_Sjm_j|SjJ'M_{J'})|SM_S\rangle|njm_j\rangle,$$

where $|SM_S\rangle$ is the core state characterized by $S=5/2$ and $M_S=\pm 5/2$, $\pm 3/2$, and $\pm 1/2$. $|njm_j\rangle$ is the hole wave function for the nth shallow hole state and $(SM_Sjm_j|SjJ'M_{J'})$ are the appropriate Clebsch-Gordan coefficients. The linear combinations for the $J'=1$ states are presented in Refs. 7, 9, and 11.

II. EXPERIMENTAL

Mn was introduced into GaAs by means of solid-state diffusion. The GaAs wafers were undoped or semi-

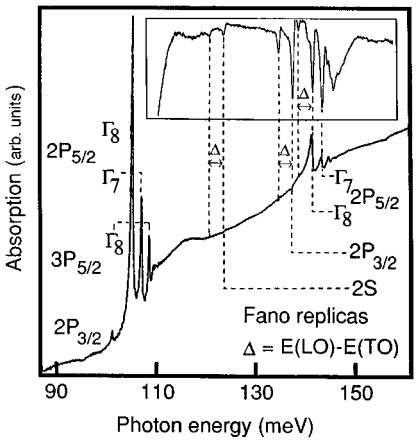

FIG. 1. Absorption and photoconductivity (inset) spectra of GaAs:Mn. The lines have been labeled according to the shallow hole states in the final state of the transitions.

insulating. Crushed Mn lumps and crushed GaAs wafers were mixed and put into a quartz ampoule together with the GaAs substrate. The ampoules were sealed in vacuum. The samples were diffused between 700 °C and 800 °C for 2–5 h. After the diffusion, the ampoules were allowed to cool in the furnace or quenched in the ambient air. Both sides of the samples were polished 10 μm and slightly etched (1 μm) in a warm (80 °C) H_2SO_4:H_2O:H_2O_2 (5:1:1) etch. About 500 μm were polished away from the surfaces of the Zeeman samples. The Ohmic contacts of the photoconductors were made either by evaporation of Zn, Au, and Cr and alloying 30 s at 550 °C or by rubbing Al-Ga contacts. The photoconductors were mounted on isolated TO-5 headers with weak adhesive to avoid strain in the sample. The transmission measurements were obtained by a BOMEM DA3.01 Fourier transform spectrometer and a LHe-cooled Ge:Cu photoconductive detector. The samples were held in a Leybold-Heareus continuous-flow cryostat at about 10 K. The uniaxial stress was applied by pressurized air via a push rod mechanism. In the Zeeman experiments, an Oxford SM-4 split coil magnet in the Voigt configuration was used, and the sample temperature was about 2 K. The maximum field used was 6.3 T.

III. NONPERTURBATION RESULTS

In Fig. 1 the absorption spectrum of Mn^0 is presented. The spectrum has already been discussed in some detail[5] and only a brief survey will be presented here. The peaks between 100 and 110 meV are due to hole excitations from the Mn^0 ground state to shallow-hole states close to the top of the valence band (see Table I). The assignment of the peaks is according to the shallow-hole states of GaAs.[12,13] By adding the theoretically obtained binding energy of the $2P_{5/2}(\Gamma_8)$ state, 7.18 meV, to the observed line energy a binding energy of 112.43 meV could be inferred, in good agreement with the 113-meV value obtained from photoluminescence.[2,3] The theoretical binding energy of the $2P_{5/2}(\Gamma_8)$ state was obtained by interpolating the data in Ref. 14 using the valence-band parameters of Refs. 12 and 13. It should be noted that different interpolation procedures can be chosen that give slightly different results.

TABLE I. Observed transition energy E_{obs} of the lines and their assigned final states. E_B^{expt} is the infrared binding energy $\Delta E = E_B^{expt} - E_{EMA}$, where E_{EMA} is the EMA-calculated binding energy. All energies are in meV.

Final state	E_{obs}	E_B^{expt}	ΔE	E_{EMA}
$2P_{3/2}(\Gamma_8)$	101.20	11.14	−0.21	11.35
$2P_{5/2}(\Gamma_8)$	105.16	7.18	0.00	7.18
$2P_{5/2}(\Gamma_7)$	107.07	5.27	−0.04	5.31
$3P_{3/2}(\Gamma_8)$				5.18
$3P_{5/2}(\Gamma_8)$	108.5	3.84	0.22	3.62
$3P_{5/2}(\Gamma_7)$				2.77
$2S_{3/2}(\Gamma_8)$		25.3	17.68	7.62
$1S_{3/2}(\Gamma_8)$		112.34	94.66	25.65

The structure at about 140 meV is due to the interaction between pseudodiscrete hole-phonon states and the valence-band continuum and is interpreted as phonon-assisted Fano resonances.[5] The resonances were also observed in photoconductivity (see the inset of Fig. 1), but the line shape and the relative intensities of the replicas are different from those observed in absorption.

The holes in the shallow bound states couple to the bulk phonon continuum. The holes are found at the Γ point in the Brillouin zone and hence the ordinary selection rule for the conservation of the crystal momentum in optical transitions ensures that the allowed transitions to excited hole-phonon states must involve the zone center LO or TO phonons. The LO and TO phonons have the energies[15] $\hbar\omega_{LO}=36.69$ meV and $\hbar\omega_{TO}=33.84$ meV ($T=4.2$ K), respectively ($\Delta_{LO\text{-}TO}=2.89$ meV). Two different series of replicas ($\Delta=2.88$ meV) are therefore above the zero-phonon lines, which was also experimentally observed (see Fig. 1).

By adding the $\hbar\omega_{LO}$ and $\hbar\omega_{TO}$ energies to the zero-phonon line energies, the $2P_{3/2}(\Gamma_8)$, $2P_{5/2}(\Gamma_8)$, and $2P_{5/2}(\Gamma_7)$ replicas are readily identified. However, an additional LO-TO doublet was detected in photoconductivity at about 120 meV. No corresponding zero-phonon line was observed either in absorption or in photoconductivity. Considering that the lowest shallow p-like states already have been accounted for and that a binding energy of about 25.3 meV can be inferred for the yet unknown electronic state it is reasonable to assign this state as the $2S_{3/2}(\Gamma_8)$ state, which is the lowest non-p-like state when excluding the $1S_{3/2}(\Gamma_8)$ state. As is noted in Table I, the energy position of the $2S_{3/2}(\Gamma_8)$ state must be lowered from the EMA value of 7.6 meV to 25.3 meV, i.e., the binding energy is increased by 17.7 meV. This may be viewed as being due to an attractive central-cell potential. It is well known that for several other deep centers with shallow excited states, e.g., the chalcogen double donors in Si, that the central-cell correction for the higher s states ($n\geq 2$) obeys a simple scaling rule. The central-cell correction is proportional to the probability of finding the excited particle at the origin, which for hydrogenic s-states is proportional to $1/n^3$. We assume that this rule also can be extended to the ground-state energy of Mn^0. The central-cell shift for the ground state will then accordingly be eight times that for the $2S$ state, i.e., $\Delta E_{1S}=141.4$ meV, which is about 47 meV larger than that experimentally observed. The $1/n^3$ scaling rule is derived from first-order

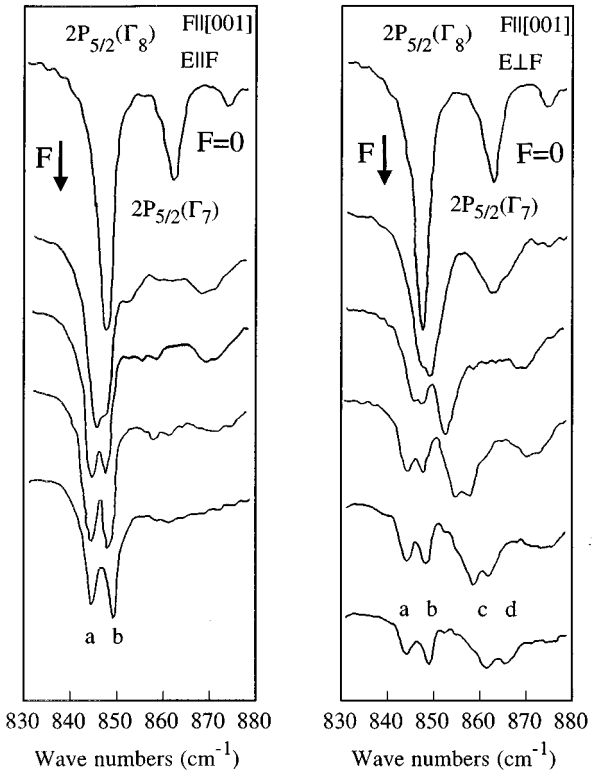

FIG. 2. Part of the uniaxial stress transmission spectra for $\mathbf{F}\|[001]$ and $\mathbf{E}\|\mathbf{F}$ and $\mathbf{E}\perp\mathbf{F}$.

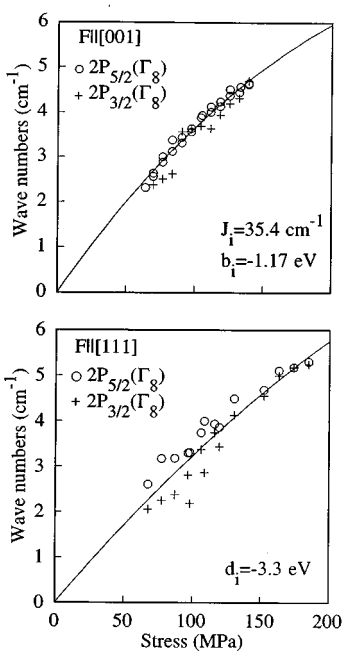

FIG. 3. Energy difference between the a and b $2P_{5/2}(\Gamma_8)$ and $2P_{3/2}(\Gamma_8)$ lines for $\mathbf{F}\|[001]$ [see Fig. 2 for the $2P_{5/2}(\Gamma_8)$ lines] and for $\mathbf{F}\|[111]$. See the text for details.

perturbation theory using hydrogenic states and will of course only be a crude approximation in this case. However, ΔE_{1S} is only about 50% larger than the experimental value and the analysis gives additional support for the assignment of the $2S$ Fano lines.

IV. UNIAXIAL STRESS RESULTS

The Mn^- core $S=5/2$ state does not show any first-order uniaxial stress splitting since it is a pure spin state. In the case of the hole, a stress splitting is generally expected when the hole resides in a Γ_8 state, but not for a Γ_6 or a Γ_7 state owing to Kramers degeneracy. The uniaxial stress Hamiltonian matrix for the Γ_8 state in T_d symmetry is given by[16]

$$\mathbf{H}_{\text{stress}}^{\Gamma_8}=a(\sigma_{xx}+\sigma_{yy}+\sigma_{zz})\mathbf{J}^2+b\left[\sigma_{xx}\left(\mathbf{J}_x^2-\frac{\mathbf{J}^2}{3}\right)+\text{c.p.}\right]$$

$$+\frac{2}{\sqrt{3}}d(\sigma_{xy}\mathbf{U}_x+\text{c.p.}),$$

where a, b, and d are deformation potentials and σ_{ij} are components of the stress tensor. $\mathbf{J}_i$ ($i=x$, y, and z) are the angular momentum matrices for a $j=3/2$ state derived from an $s=1/2$ atomic p state and $\mathbf{U}_x=(\mathbf{J}_y\mathbf{J}_z+\mathbf{J}_z\mathbf{J}_y)/2$.

Part of the uniaxial stress spectrum for the $2P_{5/2}(\Gamma_8)$ line with $\mathbf{F}\|[001]$ is presented in Fig. 2. The $2P_{5/2}(\Gamma_8)$ line is clearly resolved and splits into four components (labeled a, b, c, and d in Fig. 2). The splitting of the excited hole state can only account for two of the four observed components. The additional splitting therefore originates from a stress-induced splitting of the initial state and/or the final core state. In the Mn^-+(shallow hole) model the final core state is just that of Mn^-, i.e., $^6A_2$, which cannot split under stress. A closer examination of the stress splitting pattern reveals finer details that enable a definite assignment of the stress-split components. The intensity of the a and c lines decreases with increasing stress, whereas the opposite behavior is observed for the b and d lines. It must be pointed out that although this stress-independent intensity change is small, it has been unambiguously demonstrated since the same behavior is observed for other lines as well as for other stress directions. The measurements were carried out at a temperature of about 10 K and this behavior is most easily understood as a thermalization effect in the initial state, i.e., the ground state splits into at least two components and the population of the higher-energy state decreases with the increasing stress splitting.

The splitting attributed to the ground states was investigated in some detail to test the Mn^-+(shallow hole) model as well as to gain further insight into the ground-state properties. The energy difference between the $2P_{5/2}(\Gamma_8)$ a and b lines as well as the corresponding splitting of the other lines should then reflect the splitting of the $J'=1$ initial state. An identical splitting is also expected between the $2P_{5/2}(\Gamma_8)$ c and d lines. This is indeed experimentally observed, but due to the low intensity of the lines, the results for these two lines are not used in the analysis below.

A $J'=1$ state generally splits into two components for $\mathbf{F}\|[001]$ and [111] and three components for $\mathbf{F}\|[110]$. The splitting between the a- and b-type lines is presented in Fig. 3 for $\mathbf{F}\|[001]$ and [111] for the $2P_{5/2}(\Gamma_8)$ and $2P_{3/2}(\Gamma_8)$ lines. It is clear that the splitting for both final states is almost equal, which gives further support to our assumption that the additional splitting originates from a splitting in the initial state. Furthermore, the splitting is nonlinear for both

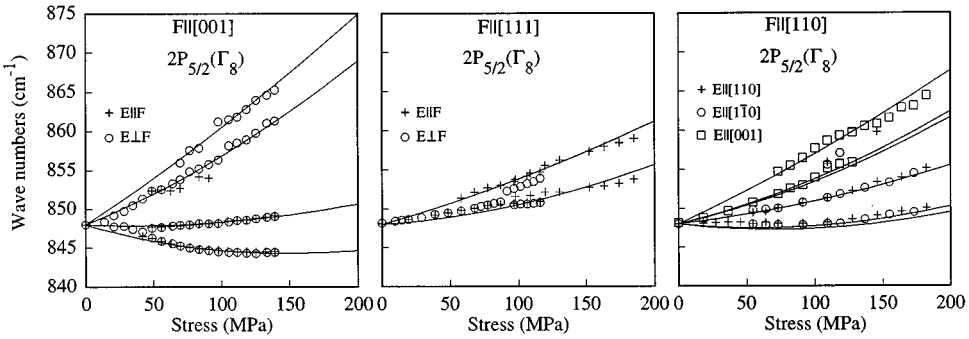

FIG. 4. Splitting of the $2P_{5/2}(\Gamma_8)$ line for **F**||[001], [111], and [110]. The full lines are obtained from a calculation based on the Mn^-+(shallow hole) model. See the text for details.

stress directions. This may be caused by a stress-induced interaction between the $J'=1$ ground state with the higher exchange split levels ($J'\geqslant 2$) in the ground-state manifold. The splitting for **F**||[001] and [111] is described by the deformation potentials b and d for the $1S_{3/2}(\Gamma_8)$ shallow hole, respectively. In order to determine b for the $1S_{3/2}(\Gamma_8)$ state as well as the exchange parameter J, the full Hamiltonian with **F**||[001] was solved numerically and J and b were determined using a standard minimization procedure. In this way the parameters were determined to be $J_i=35.4$ cm^{-1} (4.4 meV) and $b_i=-1.17$ eV (i refers to the initial state).

The splitting of the ground state for **F**||[111] is determined by J and the deformation potential d. Two fitting procedures were employed. In the first, both parameters were simultaneously fitted to the [111] data and the result was $J_i=47.5$ cm^{-1} (5.9 meV) and $d_i=-3.1$ eV. As is seen in Fig. 3, the scatter in the data is less for **F**||[001] than for **F**||[111] and it can be expected that the value found for J_i from **F**||[001] is more accurate. In the second fitting procedure for **F**||[111], the exchange parameter obtained for **F**||[001] was used and only the deformation potential d_i was calculated. The result thus obtained was $d_i=-3.3$ eV. In both cases, d_i was found to be about 3 eV, whereas the spread in J_i was substantial. However, as will be shown below, using $J_i=35.4$ cm^{-1} will give an accurate fitting to the stress splitting, which indicates that J_i is close to this value. The values found for the stress parameters of the $1S_{3/2}(\Gamma_8)$ hole coupled to the $^6A_2$ core predict an almost isotropic stress splitting of the ground state. This isotropic stress splitting pattern will simplify the identification of the stress split components for the $2P_{5/2}(\Gamma_8)$ line below.

It is interesting to note that the result for b_i and d_i is close to the values (with respect to both their absolute values as well as to their sign) previously reported for the $1S_{3/2}(\Gamma_8)$ state for the shallow acceptors C, Si, and Ge in GaAs: -0.91 and -3.8 eV, respectively.[17] This gives strong support for the Mn^-+(shallow hole) model and that the bound hole indeed has shallowlike character at least with respect to uniaxial stress perturbations.

Phonon scattering[18] and ultrasonic absorption[19] measurements have earlier revealed an excited level 2–3 meV above the Mn^0 ground state. It has been suggested[9] that this level was the $J=2$ level. However, our energy determined for $J_i\approx 4.5$–6 meV predicts that the $J=2$ levels are to be found at 9–12 meV above the ground state. Attempts to observe the 2–3 meV excited state in absorption by thermal population of the excited state have failed and on the basis of our data the origin of this excited level observed in phonon scattering remains unclear.

In Fig. 4 the stress splitting for the $2P_{5/2}(\Gamma_8)$ line for stress in the three main stress directions [001], [111], and [110] is presented together with the splitting predicted by the model (full lines). As is clearly seen, the fitting satisfactory reproduces the experimental splitting when using $J_i=35.4$ cm^{-1}, $b_1=-1.17$, and $d_i=-3.3$ eV for the $1S_{3/2}(\Gamma_8)$ initial shallow-hole state. As mentioned above, the ground state splits almost isotropically and we can readily identify in Fig. 4 the splitting that originates from the initial and final states of the transitions, respectively.

For **F**||[001] the $2P_{5/2}(\Gamma_8)$ line splits into four components and a direct comparison with the **F**||[111] splitting pattern reveals that the four components can be grouped to-

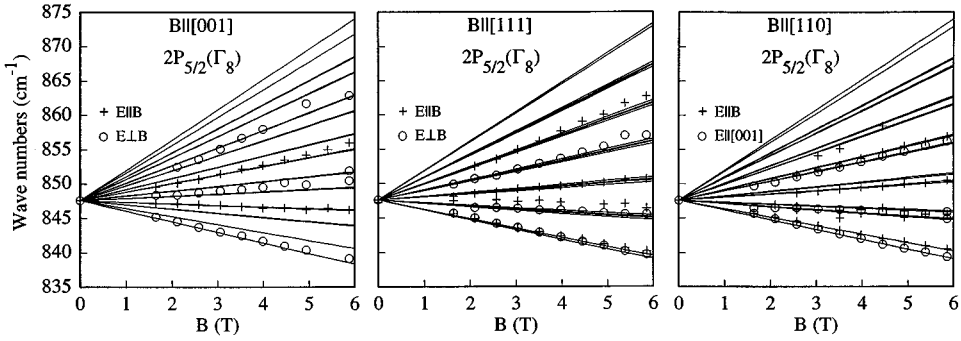

FIG. 5. Zeeman splitting of the $2P_{5/2}(\Gamma_8)$ line for **B** parallel to [001], [111], and [110]. The full lines are obtained from a calculation based on the Mn^-+(shallow hole) model. See the text for details.

gether in two groups of two lines each, showing the same relative splitting as the two lines for $\mathbf{F}\|[111]$. A closer examination of the $\mathbf{F}\|[110]$ data shows that also in this case the $2P_{5/2}(\Gamma_8)$ line splits into two groups containing two lines, and the latter two show almost the same splitting as observed for the other directions due to the initial state splitting. An additional splitting is predicted by our calculations for $\mathbf{F}\|[110]$ (Fig. 4). It is due to a splitting of the $\mathbf{M}_{J'}=\pm 1$ ground state, but is too small to be experimentally detected. From the splitting of the $2P_{5/2}(\Gamma_8)$ line the deformation potentials b and d of the final $2P_{5/2}(\Gamma_8)$ shallow-hole state can be determined. b was calculated from the $2P_{5/2}(\Gamma_8)$ $\mathbf{F}\|[001]$ data and d from the $\mathbf{F}\|[111]$ data. In this way the deformation potentials were determined and the results were $b=0.49$ eV, and $d\approx 0$ eV. The sign of the deformation potential b for the $2P_{5/2}(\Gamma_8)$ final state could not be determined from stress splitting solely. However, the polarization results and the corresponding calculations presented below for both the uniaxial stress and the Zeeman experiments unambiguously determine b to be positive. It should be noted that a small possible additional splitting might be inferred from the $\mathbf{F}\|[111]$ data as seen in Fig. 4. However, we are convinced that this small difference in the $\mathbf{E}\|\mathbf{F}$ and $\mathbf{E}\perp\mathbf{F}$ data is an artifact due to inhomogeneous stress applied to the sample. This is also supported by the good fit using these values for $\mathbf{F}\|[110]$ (Fig. 4) and a comparison with previous results for the Cu acceptor in GaAs.[20]

Only the difference between the hydrostatic deformation potentials for the final and initial state can be determined in the stress experiments and the fitting to the data gives $\Delta a = a_f - a_i = -0.65$ eV. The hydrostatic shift in the initial state is determined by the shift in the subsystems, i.e., the Mn^- core and the $1S_{3/2}(\Gamma_8)$ hole. The Mn^- core state is the same for both the initial and final state and no contribution to the hydrostatic shift is expected from the core state. If the $1S_{3/2}(\Gamma_8)$ hole is indeed purely effective-mass-like, both hole states in the transitions, $1/S_{3/2}(\Gamma_8)$ and $2P_{5/2}(\Gamma_8)$, should show the same hydrostatic shift. Since a substantial shift nevertheless is observed, it is tempting to ascribe this shift due to a non-effective-mass character of the ground-state hole.

V. ZEEMAN RESULTS

The $S=5/2$ core states split in a magnetic field isotropically according to $\mathbf{H}^{5/2}_{\text{Zeeman}}=\mu_B g_S \mathbf{B}\cdot\mathbf{S}$, where g_S is close to the free spin g factor of about 2, μ_B is the Bohr magnetron, and $\mathbf{B}$ is the applied field. The two hole doublets Γ_6 and Γ_7 split according to $\mathbf{H}^{1/2}_{\text{Zeeman}}=\mu_B g_j \mathbf{B}\cdot\mathbf{j}$, where g_j is different for different hole states and $\mathbf{j}$ could be taken as the three $s=1/2$ spin matrices.

The direct produce $\Gamma_8\otimes\Gamma_8$ contains two T_1 irreducible representations and therefore two parameters g_1' and g_2' are needed to describe the Zeeman splitting of the general Γ_8 state. The Zeeman Hamiltonian matrix takes the form[21]

$$\mathbf{H}^{\Gamma_8}_{\text{Zeeman}}=\mu_B\{g_1'\mathbf{B}\cdot\mathbf{J}+g_2'(B_x\mathbf{J}_x^3+B_y\mathbf{J}_y^3+B_z\mathbf{J}_Z^3)\}.$$

In fitting our experimental data to the theory outlined here we use as basis functions the simple product functions $|SM_S\rangle|njm_j\rangle$ and numerically solved the exchange and perturbation Hamiltonian simultaneously. The total Zeeman Hamiltonian matrix for, e.g., a Γ_8 hole state coupled to the $S=5/2$ core could then conveniently be written as

$$\mathbf{H}=J\mathbf{S}\otimes\mathbf{J}+\Pi_6\otimes\mathbf{H}^{\Gamma_8}_{\text{Zeeman}}+\mathbf{H}^{5/2}_{\text{Zeeman}}\otimes\Pi_4,$$

where Π_Π is an $n\times n$ unit matrix and $\otimes$ is the tensor product.

The g factor for the $J=1$ ground state may easily be derived and one finds $g=7/4g_S-3/4g_1'-123/80g_2'$. Schneider *et al.*[9] calculated g for the $J=1$ ground state using the g values of the Sn acceptor of $g_1'=+0.78$ and $g_2'=0.07$ and $g_S=2.003$. The calculated value was $g=2.78$ (note the numerical error in Ref. 9), in almost perfect agreement with the experimental value of 2.77.

The Zeeman splitting of the $2P_{5/2}(\Gamma_8)$ line is presented in Fig. 5, as well as the fitting according to the Mn^-+(shallow hole) model. For the $1S_{3/2}(\Gamma_8)$ ground-state hole, the g values for the Sn acceptor were used in the fitting. For the final $2P_{5/2}(\Gamma_8)$ state, very good agreement was obtained using the theoretical values in Refs. 22 and 23 of $g_1'=-3.15$ and $g_2'=1.57$. For all directions of the magnetic field, transitions to the higher Zeeman components were not detected. This may easily be explained by noting that the measurements were carried out at $T=1.9$ K, which was sufficiently low to only have population of the lowest Zeeman component in the initial state, i.e., the $J'=1$, $M_{J'}=-1$ state. The $J'=1$, $M_{J'}=-1$ state contains only $S=5/2$ states from $M_S=-5/2$ up to 3/2. Since the M_S value is conserved in the transitions those four final states associated with the $M_S=5/2$ final core

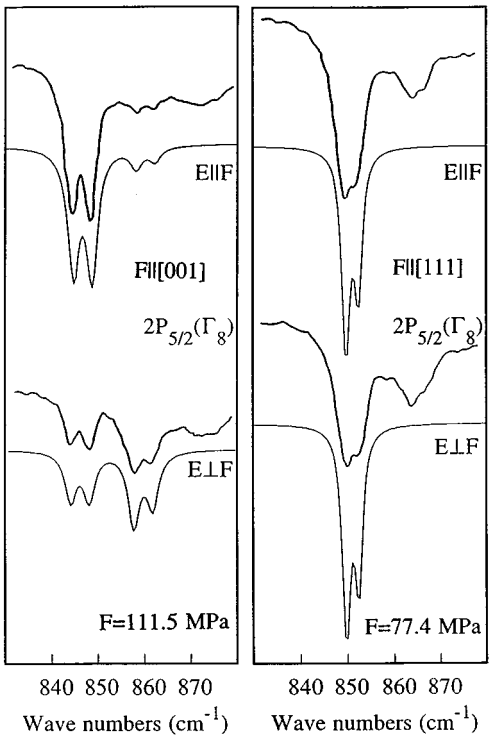

FIG. 6. Calculated intensities (lower spectra) for the $2P_{5/2}(\Gamma_8)$ line for $\mathbf{F}\|[001]$ and $\mathbf{F}\|[111]$ compared with the experimental results (upper spectra). The broad high-energy feature is due to the $2P_{5/2}(\Gamma_7)$ line.

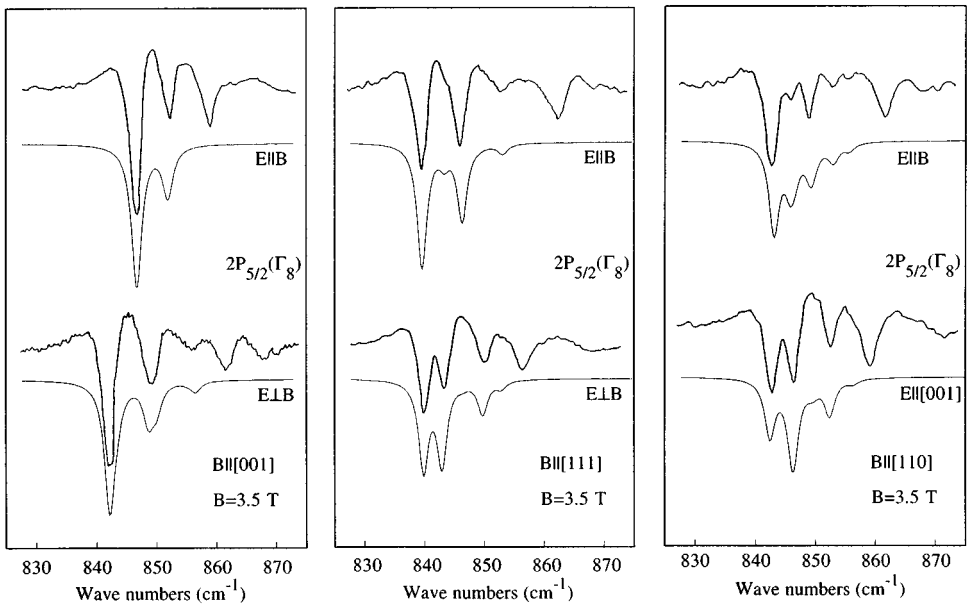

FIG. 7. Comparison between the experimental (upper spectra) and calculated (lower spectra) Zeeman intensities for the $2P_{5/2}(\Gamma_8)$ line. The lines close to 860 cm^{-1} and at higher energies are due to transition to the $2P_{5/2}(\Gamma_7)$ line.

state can never be reached in electric-dipole transitions. Furthermore, only 5% of the initial $J'=1$, $M_{j'}=-1$ state is associated with $M_S=3/2$ and these four transitions are expected to be weak.

VI. POLARIZATION RESULTS

The polarization selection rules were also calculated. The electric-dipole matrix **Q** for Γ_8 to Γ_8 transitions can conveniently be written[21]

$$\mathbf{Q}^{\Gamma_8\text{-}\Gamma_8}=-\frac{2}{\sqrt{3}}(D+D')\mathbf{U}-\frac{4i}{\sqrt{3}}D'\mathbf{V},$$

where **U** are the matrices described above, **V** is defined by $\mathbf{V}_x=\frac{1}{2}[\mathbf{J}_x\cdot(\mathbf{J}_y^2-\mathbf{J}_z^2)+(\mathbf{J}_y^2-\mathbf{J}_z^2)\cdot\mathbf{J}_x]$, and D and D' are two complex parameters, in general, that are given in all four parameters. The transition probabilities are determined by the squared absolute values of the components of $\mathbf{Q}^{\Gamma_8\text{-}\Gamma_8}$ and the common phase factor of D and D' can be neglected. We can therefore choose $D=\alpha$ and $D'=\beta e^{i\varphi}$, where α and β are real positive numbers. The sum of the transition probabilities from all initial states to, e.g., all $2P_{5/2}(\Gamma_8)$ final states can be normalized for each polarization[21] and we obtain

$$4|D+D'|^2+16|D'|^2=4\alpha^2+8\alpha\beta\cos\varphi+20\beta^2=4N';$$

only two free parameters remain as demanded by group-theoretical arguments for Γ_8 to Γ_8 transitions. In the limits $\beta=0$ and $\alpha=0$ one gets $\alpha=\sqrt{N'}$ and $\beta=\sqrt{N'/5}$, respectively. By choosing different $\cos\varphi$ in the range $-1\leqslant\cos\varphi\leqslant 1$ we can, e.g., solve for β as a function of α,

$$\beta=\frac{-\alpha\cos\varphi}{5}\pm\frac{1}{5}\sqrt{5N'-\alpha^2(6-\cos^2\varphi)},\qquad \beta\geqslant 0.$$

Each element of the matrix **Q** can be expressed in terms of α and β. The unique set of α and β belonging to every nonperturbed line is determined by a fit to the experimental data.

The $2P_{5/2}(\Gamma_8)$ line shows strong polarization selections rules for **F**||[001]. The fitted intensities for **F**||[001] and **F**||[111] using $\alpha=0.38$ and $\beta=0.08$ are compared with the experimental results in Figs. 6 and 7. Using the same α and β, the intensity for different stress directions and polarizations could easily be calculated. Good agreement was obtained, which gives further support for the correctness of the model.

The measured intensities of the $2P_{5/2}(\Gamma_8)$ Zeeman lines as well as the calculated ones are presented in Fig. 7. The intensity parameters α and β used here are the same as for uniaxial stress. Very good agreement between experiment and theory was obtained for **B**||[001] and **B**||[111], whereas a small deviation was detected for **B**||[110]. However, this could easily be explained by a small error in the B field axis and/or in the photon **k** vector. The Zeeman and stress spectra were calculated using a Lorentzian line shape and a line width at half maximum of 2.1 cm^{-1}.

VII. SUMMARY

The GaAs:Mn excitation spectrum has been investigated in detail by employing uniaxial stress and Zeeman spectroscopy. All our experimental findings are fully in accordance with the Mn^-+(shallow hole) model.

ACKNOWLEDGMENTS

The authors acknowledge financial support from lthe Swedish Natural Science Research Foundation, the Board for Industrial and Technical Development, and the Swedish Research Council for Engineering Sciences.

*Present address: the Royal Institute of Technology, Solid State Electronics, P.O. Box E229, S-164 40 Kista, Sweden.

[1] L. J. Vieland, J. Appl. Phys. **33**, 2007 (1962).
[2] T. C. Lee and W. W. Anderson, Solid State Commun. **2**, 265 (1964).
[3] W. Schairer and M. Schmidt, Phys. Rev. B **10**, 2501 (1974).
[4] R. A. Chapman and W. G. Hutchinson, Phys. Rev. Lett. **18**, 443 (1967).
[5] M. Kleverman, E. Janzén, M. Linnarsson, and B. Monemar, in Impurities, Defects, and Diffusion in Semiconductors: Bulk and Layered, edited by D. J. Wolford, I. Bernhule, and E. E. Haller, MRS Symposia Proceedings No. 163 (Materials Research Society, Pittsburgh, 1990), p. 207.
[6] L. Montelius, S. Nilsson, L. Samuelson, E. Janzén, and M. Ahlström, J. Appl. Phys. **64**, 1564 (1988).
[7] N. Almeleh and B. Goldstein, Phys. Rev. **128**, 1568 (1962).
[8] R. Bleekrode, J. Dieleman, and H. J. Vegter, Phys. Lett. **2**, 355 (1962).
[9] J. Schneider, U. Kaufmann, W. Wilkening, M. Baeumler, and F. Köhl, Phys. Rev. Lett. **59**, 240 (1987).
[10] M. Baeumler, B. K. Meyer, U. Kaufmann, and J. Schneider, Mater. Sci. Forum **38–41**, 797 (1989).
[11] E. U. Condon and G. H. Shortley, *The Theory of Atomic Spectra* (Cambridge University Press, Cambridge, 1963), p. 76.
[12] A. Baldereschi and N. O. Lipari, Phys. Rev. B **8**, 2697 (1973).
[13] A. Baldereschi and N. O. Lipari, Phys. Rev. B **9**, 1525 (1974).
[14] M. Said, M. A. Kanehisa, M. Balkanski, and Y. Saad, Phys. Rev. B **35**, 687 (1987).
[15] A. Mooradian and G. B. Wright, Solid State Commun. **4**, 431 (1966).
[16] E. P. Kartheuser, S. Rodriguez, and P. Fisher, Phys. Status Solidi B **64**, 11 (1974).
[17] M. Schmidt, Ph.D. thesis, Universität Stuttgart (unpublished).
[18] A. de Combarieu and K. Lassmann, in *Phonon Scattering in Solids*, edited by L. J. Challis, V. W. Rampton, and A. F. G. Wyatt (Plenum, New York, 1976).
[19] K. Lassmann and Hp. Schad, Solid State Commun. **18**, 449 (1976).
[20] E. Janzén, M. Linnarsson, B. Monemar, and M. Kleverman, in *Impurities, Defects and Diffusion in Semiconductors: Bulk and Layered* (Ref. 5) p. 169.
[21] A. K. Bhattacharjee and S. Rodriguez, Phys. Rev. B **6**, 3836 (1972).
[22] R. Atzmüller, M. Dahl, J. Kraus, G. Schaak, and J. Schubert, J. Phys.: Condens. Matter **3**, 6775 (1991).
[23] W. O. G. Schmitt, E. Bangert, and G. Landwehr, J. Phys.: Condens. Matter **3**, 6789 (1991).